energies

MDPI

Article

Numerical Simulation Investigation on the Windage Power Loss of a High-Speed Face Gear Drive

Yu Dai [1,2,*], Feiyue Ma [1,2], Xiang Zhu [1,2] and Jifu Jia [1,2]

1 College of Mechanical and Electrical Engineering, Central South University, Changsha 410083, China; feiyuema@csu.edu.cn (F.M.); zhuxiang2017@csu.edu.cn (X.Z.); jifujia@csu.edu.cn (J.J.)
2 State Key Laboratory of High Performance Complex Manufacturing, Central South University, Changsha 410083, China
* Correspondence: 210143@csu.edu.cn

Received: 3 May 2019; Accepted: 30 May 2019; Published: 31 May 2019

Abstract: Reducing the energy consumption and improving the efficiency of high-speed transmission systems are increasingly common goals; the windage power loss is not negligible in these methods. In this work, the multi-reference frame (MRF) and periodic boundary conditions (PBC) based on the computational fluid dynamics (CFD) method were adopted to investigate the windage phenomena of a single face gear with and without a shroud, and the impact of the gear speed on the windage power loss was analyzed. Furthermore, the effects on the distribution of static pressure due to the distances between the shroud and the gear body in different directions, including the outer radius direction, the inner radius direction, and the addendum direction were investigated. The results indicate that the gear speed significantly affected the windage loss, as the higher the gear speed was, the greater the windage power loss. Additionally, the shroud could effectively reduce the windage power loss, where the optimal distance from the addendum to the shroud was not the minimum distance; however, for the distances from the shroud to the inner radius and the outer radius, the smaller the distance was, the smaller the windage loss. The results can provide a theoretical basis and technical reference for reducing the windage power loss of various face gear drives.

Keywords: windage power loss; high-speed face gear; multi-reference frame (MRF); periodic boundary conditions (PBC); shroud; computational fluid dynamics (CFD)

1. Introduction

All rotating machinery will stir up the surrounding air, resulting in windage power loss, restricting fuel economy and reducing transmission efficiency, especially for aeronautical transmission systems. The face gear drive is a new kind of meshing transmission between a cylindrical gear and a bevel gear, which has been successfully applied in the main reducer of armed helicopters owing to its numerous advantages [1–4]. Although the efficiency of a well-designed gearbox can reach 99%, the power loss cannot be neglected in high-power applications. Due to the working conditions under ultra-high speed, the contact area between the face gear and the surrounding air increases, which intensifies the pressure difference between the tooth surfaces and produces a resistance moment opposite to the face gear's rotation; all of these factors will lead to the increase of the windage power loss of face gears. Additionally, windage can be a major source of the heat produced and can dominate other losses [5,6]. Hence, it is necessary to investigate the windage power loss of the face gear rotating in the air and explore effective methods to reduce energy loss, so as to improve the performance and expand the engineering application of the face gear drives.

Recently, certain progress has been made in research on windage power loss of gears. In the early period, due to the immaturity of computer methods, the windage loss could only be studied through

experiments and theories. Dawson [7,8] conducted multiple experiments to study the influencing factors of the windage power loss of spur gears, and these studies yielded a rough empirical formula. Anderson et al. [9,10] proposed a method for calculating the windage power loss and analyzed the influences of size, pitch, width, and ratio of the spur gear on the losses. According to Dawson's and Anderson's works, Diab et al. [11] presented two approaches to predict the windage losses of spur gears based on a series of preliminary experimental and theoretical results, and they proposed formulas for the two approaches. In addition, Handschuh et al. [12] and Farrall et al. [13] compared the experimental and theoretical results of windage losses of helical gears and spiral bevel gears, respectively, and they finally obtained the factors affecting the transmission efficiency. Subsequently, Eastwick et al. [14] reviewed experimental studies of spur gears, helical gears, spiral bevel gears, and existing windage power loss models, and they provided a comprehensive explanation of windage loss. Johnson et al. [15] studied the windage loss of unmeshed spiral bevel gears rotating in air, and they came to the conclusion that the windage power loss of clockwise rotation is greater than that of anticlockwise rotation.

With the rapid development of computational fluid dynamics (CFD) technology in recent years, CFD numerical simulation is increasingly being used to investigate the windage loss of gears, to acquire more comprehensive windage information and to reduce research costs. Hill et al. [16] applied the CFD method to investigate the influence of the gear structure on the windage losses with and without a shroud, and they compared the results with the experimental data to verify the numerical value and modeling method. Compared with the experimental results, the MRF approach based on the CFD has been proven to effectively predict the power loss of ordinary gear transmissions [17], and this approach was also applicable to the multiphase problems [18]. Pallas et al. [19] presented a correlation method based on the classical approach through the CFD method for estimating the windage power loss, and they finally pointed out that the volume flow rate significantly affects the windage power loss of spur gears. To reduce windage power loss of spiral bevel gears in an aeroengine transmission system, Arisawa et al. [20] developed the windage power loss through CFD simulations and put forward a method for improving the effectiveness of the shroud. Based on the experimental results and CFD simulations, Voeltzel et al. [21] studied the windage loss of rotating helical gears; their results indicated that both tooth width and helical angle have an effect on the windage loss. A single-phase computational research study was performed by Rapley et al. [22] for investigating the influence of clockwise and anticlockwise rotation and boundary walls on windage losses of spiral bevel gears with or without shroud. Marchesse et al. [23] applied CFD code to conduct two-dimensional and three-dimensional numerical simulations of the windage loss in pure air, and they compared the results with a special experiment. To reduce the dissipated power, Concli et al. [24] applied the CFD method to predict the power loss generated by a single rotating gear and a meshing gear pair, and developed an innovative calculation method to quantify the efficiency and the related operating temperatures under different working conditions [25]. Delgado et al. [26] analyzed the experimental and theoretical results of windage power loss with and without a shroud, pointing out that a shroud can significantly reduce the windage loss of spur gears. Seetharaman et al. [27] proposed a simplified hydrodynamic model for predicting the windage losses under the condition of oil jet lubrication and compared the predicted results with the existing empirical formulas of spur gears to evaluate the accuracy of the model. Webb et al. [28] investigated the relationship between the teeth and windage loss of spiral bevel gears with a shroud based on the parameterized solid model and CFD method, and they showed that the more teeth, the smaller the windage loss. Under the conditions of different gear speeds and various shrouds, the windage loss of spur gears rotating in the air with oil particles was studied by the CFD method, and the influence of oil droplets on the windage loss was quantitatively studied [29]. Besides, to reduce the solving time of the numerical simulation, a new strategy of an automatic mesh generation in the CFD was developed to simulate the windage phenomenon. The simulation results were in good agreement with the experimental data, validating the correctness of the method [30,31].

However, there are few studies on the windage power loss of face gears, which greatly limits their performance promotion and engineering application. Considering this condition, in this paper, CFD

numerical simulation was applied to investigate the windage power loss of a face gear rotating in the air. The study included the following three parts: First, the tooth profile of the face gear through the tooth surface equation was introduced. Then, the CFD numerical approaches, including governing equations, calculation model, and main settings, were finished. Finally, the influence of gear speed and the distance between the gear body and the shroud on windage power loss were investigated, and the shroud that could most effectively reduce windage power loss of the face gear drive was recommended.

2. Methods of Calculating the Tooth Surface Equation and Conducting Simulations

2.1. Tooth Surface Equation

Windage power loss is defined as the energy loss caused by the friction between the rotating tooth surface and the surrounding gas medium [29,32]. Hence, the tooth surface shape of a face gear should be considered first through the theoretical equation. The flowchart of establishing face gear tooth surface equations is shown in Figure 1.

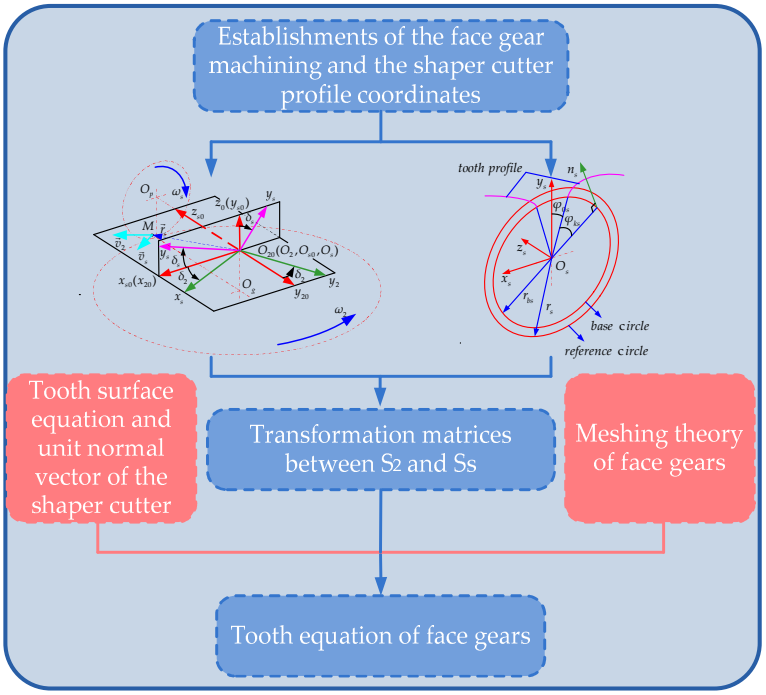

Figure 1. Flowchart of establishing face gear tooth surface equations.

Regardless of the installation error, the shaper cutter tooth profile and the face gear machining coordinates are illustrated in Figure 2a,b, respectively.

$S_{s0}(x_{s0}, y_{s0}, z_{s0})$, $S_s(x_s, y_s, z_s)$, $S_{20}(x_{20}, y_{20}, z_{20})$, and $S_2(x_2, y_2, z_2)$ indicate the fixed coordinate system of the shaping cutter, the rotation coordinate system of the shaping cutter, the fixed coordinate system of the face gear, and the rotation coordinate system of the face gear, respectively. r_{bs} and r_s are the base circle radius and the reference circle radius of the shaper cutter, respectively; n_s denotes the unit normal vector of the shaper cutter tooth profile; φ_{0s} denotes the angle between the line from the midpoint of the alveolar to point O_s and the line between the starting point of the involute and point O_s; φ_{ks} is the central angle between the starting point of the involute and the tangent point between the normal vector and the basic circle at any point of the involute; δ_s and δ_2 are the rotation angles of the shaper cutter and the face gear, respectively; and $O_{20}(O_2, O_s, O_{s0})$ is the intersection point of the axis of the shaper cutter and the face gear.

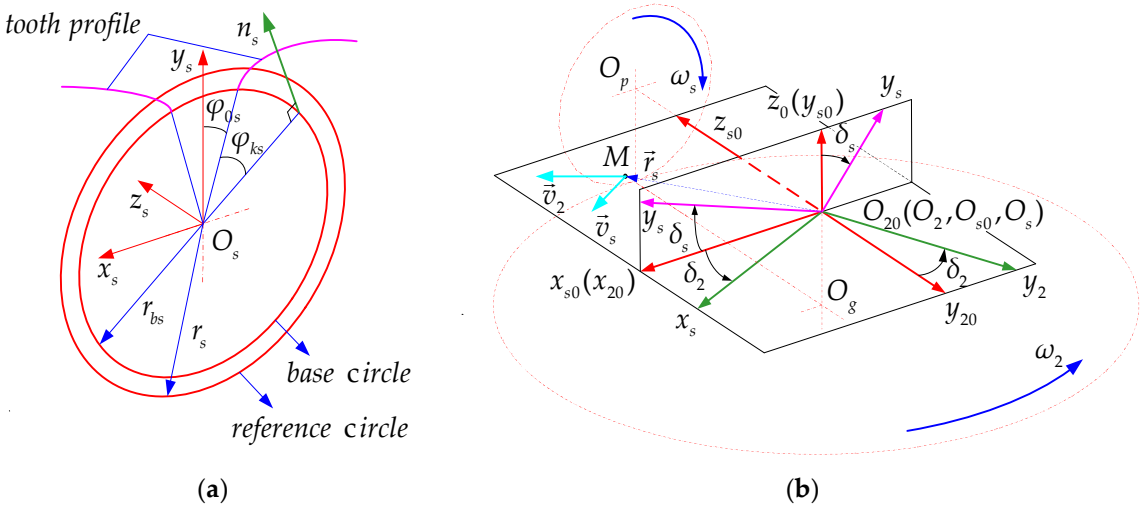

Figure 2. (**a**) Tooth profile of the shaper cutter; (**b**) machining coordinates of the face gear pair.

According to Litvin's and Guingand's [33–35] investigations, the tooth surface equation and unit normal vector of the shaper cutter are calculated through Equations (1) and (2), respectively:

$$\vec{r}_s = \begin{bmatrix} \pm r_{bs}[\sin(\varphi_{0s}+\varphi_{ks}) - \varphi_{ks}\cos(\varphi_{0s}+\varphi_{0s})] \\ -r_{bs}[\cos(\varphi_{0s}+\varphi_{ks}) + \varphi_{ks}\sin(\varphi_{0s}+\varphi_{0s})] \\ \varpi_s \end{bmatrix}, \tag{1}$$

$$\vec{n}_s = \frac{(\partial r_s/\partial\varphi_{ks})\cdot(\partial r_s/\partial v_s)}{\left|(\partial r_s/\partial\varphi_{ks})\cdot(\partial r_s/\partial v_s)\right|} = \begin{bmatrix} \mp\cos(\varphi_{0s}+\varphi_{0s}) \\ -\sin(\varphi_{0s}+\varphi_{0s}) \\ \varpi_s \end{bmatrix}, \tag{2}$$

where ϖ_s is the tooth width parameter in the z-axis direction.

According to Figure 2b, the transformation matrices between coordinate systems S_{20}, S_2, S_{s0}, and S_s are as follows:

$$S_{20} \to S_2 = \begin{bmatrix} \cos\delta_2 & -\sin\delta_2 & 0 \\ \sin\delta_2 & \cos\delta_2 & 0 \\ 0 & 0 & 1 \end{bmatrix}, \tag{3}$$

$$S_{20} \to S_{s0} = \begin{bmatrix} 1 & 0 & 0 \\ 0 & 0 & -1 \\ 0 & 1 & 0 \end{bmatrix}, \tag{4}$$

$$S_{s0} \to S_s = \begin{bmatrix} \cos\delta_s & -\sin\delta_s & 0 \\ \sin\delta_s & \cos\delta_s & 0 \\ 0 & 0 & 1 \end{bmatrix}, \tag{5}$$

Thus, the relationship between the rotation coordinate system of the shaper cutter and the rotation coordinate system of the face gear can be obtained by the following Equation (6):

$$S_2 \to S_s = (S_{20} \to S_2)^{-1}\cdot(S_{20} \to S_{s0})\cdot(S_{s0} \to S_s) = \begin{bmatrix} \cos\delta_2\cos\delta_s & -\cos\delta_2\sin\delta_s & -\sin\delta_2 \\ -\sin\delta_2\cos\delta_s & \sin\delta_2\sin\delta_s & -\cos\delta_2 \\ \sin\delta_s & \cos\delta_s & 0 \end{bmatrix}, \tag{6}$$

According to the spatial meshing theory of the face gear, the relationship between the tooth surface equation of the face gear and the tooth equation of the shaper cutter satisfies the following equation:

$$\vec{r}_2 = (S_2 \to S_s) \cdot \vec{r}_s = \begin{bmatrix} \cos\delta_2 \cos\delta_s & -\cos\delta_2 \sin\delta_s & -\sin\delta_2 \\ -\sin\delta_2 \cos\delta_s & \sin\delta_2 \sin\delta_s & -\cos\delta_2 \\ \sin\delta_s & \cos\delta_s & 0 \end{bmatrix} \cdot \vec{r}_s, \tag{7}$$

It is known that the unit normal vector at any point on the gear tooth surface is perpendicular to the velocity direction of the point. Suppose that there is an arbitrary contact point $M(x_s, y_s, z_s)$ on the tooth surface of the shaper cutter in the rotation coordinate system S_s; as shown in Figure 2b, the unit normal vector is $\vec{n}_s$, and the position vector is $\vec{r}_s$. The velocity $\vec{v}_s$ and $\vec{v}_2$ (shown in Figure 2b) of contact point M in the rotation coordinate systems S_s and S_2 can be expressed as:

$$\begin{cases} \vec{v}_s = \vec{\omega}_s \times \vec{r}_s \\ \vec{v}_2 = \vec{\omega}_2 \times \vec{r}_s \end{cases}, \tag{8}$$

The matrix representation of velocity $\vec{v}_s$ is shown below:

$$\vec{\omega}_s = \begin{bmatrix} 0 & 0 & \omega_s \vec{k}_s \end{bmatrix}^T, \tag{9}$$

The relationship between $\vec{\omega}_s$ and $\vec{\omega}_2$ can also be calculated by the transformation matrix

$$\vec{\omega}_2 = (S_2 \to S_s) \cdot \vec{\omega}_s, \tag{10}$$

By combining Equations (8)–(10), the relative velocity of the contact point M in the rotation system S_s can be obtained. Since the relative velocity is perpendicular to the unit normal vector $\vec{n}_s$ at the contact point M, their dot product is 0.

$$\vec{n}_s \cdot (\vec{v}_s - \vec{v}_2) = 0, \tag{11}$$

By substituting Equations (2) and (7)–(10) into Equation (11), the matrix form of the tooth surface equation of the face gear is shown as the following equation:

$$\vec{r}_2 = \begin{bmatrix} r_{bs}\left[\cos\delta_2(\sin\theta \mp \varphi_{ks}\cos\theta) - \frac{\omega_s \sin\delta_2}{\omega_2 \cos\theta}\right] \\ -r_{bs}\left[\sin\delta_2(\sin\theta \mp \varphi_{ks}\cos\theta) + \frac{\omega_s \cos\delta_2}{\omega_2 \cos\theta}\right] \\ -r_{bs}(\cos\theta \pm \varphi_{ks}\sin\theta) \end{bmatrix}, \tag{12}$$

where θ denotes the relationship among δ_s, φ_{0s}, and φ_{ks}, that is $\theta = \delta_s \pm (\varphi_{0s} + \varphi_{ks})$. According to Equation (12), it can be known that the tooth surface of the face gear is symmetrical in the direction of the outer radius of the face gear, as shown in Figure 3. Therefore, it can be concluded that the rotation direction of the face gears has no effect on the windage power loss.

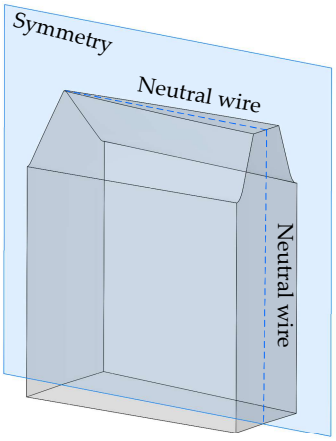

Figure 3. Symmetry of the face gear tooth surface.

2.2. Fluid Governing Equation

Any fluid flows in CFD simulations meet three basic governing equations of fluid mechanics, including the continuity equation, the momentum equation, and the energy equation [36–38], which can be respectively expressed as Equations (13), (14), and (15):

$$\frac{\partial \rho}{\partial t} + \frac{\partial(\rho \vec{u})}{\partial x} + \frac{\partial(\rho \vec{v})}{\partial y} + \frac{\partial(\rho \vec{w})}{\partial x} = 0, \tag{13}$$

$$\begin{cases} \rho \frac{d\vec{u}}{dt} = \rho F_{bx} + \frac{\partial \vec{p}_{xx}}{\partial x} + \frac{\partial \vec{p}_{yx}}{\partial y} + \frac{\partial \vec{p}_{zx}}{\partial z} \\ \rho \frac{d\vec{v}}{dt} = \rho F_{by} + \frac{\partial \vec{p}_{xy}}{\partial x} + \frac{\partial \vec{p}_{yy}}{\partial y} + \frac{\partial \vec{p}_{zy}}{\partial z} \\ \rho \frac{d\vec{w}}{dt} = \rho F_{bz} + \frac{\partial \vec{p}_{xz}}{\partial x} + \frac{\partial \vec{p}_{yz}}{\partial y} + \frac{\partial \vec{p}_{zz}}{\partial z} \end{cases}, \tag{14}$$

$$\frac{\partial(\rho E)}{\partial t} = \frac{\partial}{\partial x}\left(\frac{\varepsilon}{c_k}\frac{\partial T}{\partial x}\right) + \frac{\partial}{\partial y}\left(\frac{\varepsilon}{c_k}\frac{\partial T}{\partial y}\right) + \frac{\partial}{\partial z}\left(\frac{\varepsilon}{c_k}\frac{\partial T}{\partial z}\right) + S_h, \tag{15}$$

where ρ represents the fluid density, t denotes the time; u,v, and w indicate the velocity components in the directions of the coordinate systems; p is the pressure on the fluid microelement; F_{bx}, F_{by}, and F_{bz} refer to the unit mass forces in the directions of the coordinate axes; p_{xx}, p_{yx}, p_{zx}, etc., are the components of viscous stress acting on the surface of the fluid microelement; E indicates the total energy of the fluid microelement; c_k denotes the specific heat capacity; T refers to the total temperature; ε denotes the heat transfer coefficient of the fluid, and S_h represents the viscosity dissipation term and satisfies the following equation:

$$S_h = \mu\left[2\left(\frac{\partial u}{\partial x}\right)^2 + 2\left(\frac{\partial v}{\partial y}\right)^2 + 2\left(\frac{\partial w}{\partial z}\right)^2 + \left(\frac{\partial u}{\partial y} + \frac{\partial v}{\partial x}\right)^2 + \left(\frac{\partial u}{\partial z} + \frac{\partial w}{\partial x}\right)^2 + \left(\frac{\partial v}{\partial z} + \frac{\partial w}{\partial y}\right)^2\right], \tag{16}$$

Due to the high rotation speed of the gear and the complexity of the tooth shape, there will be strong swirling flow during the rotation process; thus, a low-Reynolds number turbulent model, the shear stress transport (SST) $k-\omega$ model, is applied to more accurately describe the drag and separation effects of the tooth surface on the air flow according to reference [5,19]. When the SST $k-\omega$ model is used with coarser mesh, the low-Reynolds $k-\omega$ model in the near wall is switched to the high-Reynolds $k-\varepsilon$ model in the far wall. The relationship can be expressed as:

$$\begin{cases} \frac{\partial(\rho k)}{\partial t} + \frac{\partial(\rho k u_i)}{\partial x_i} = \frac{\partial}{\partial x_j}\left(\Gamma_k \frac{\partial k}{\partial x_j}\right) + G_k - Y_k + S_k \\ \frac{\partial(\rho \varepsilon)}{\partial t} + \frac{\partial(\rho \varepsilon u_i)}{\partial x_i} = \frac{\partial}{\partial x_j}\left(\Gamma_\omega \frac{\partial \omega}{\partial x_j}\right) + C_\omega - Y_\omega + C_\omega + S_\omega \end{cases}, \tag{17}$$

where G_k is the kinetic energy of turbulence; G_ω indicates the equation associated with ω; Γ_k and Γ_ω refer to the effective diffusion terms of k and ω, respectively; Y_k and Y_ω represent the effective diffusion terms of k and ω, respectively; C_ω denotes the orthogonal divergent term; S_k and S_ω refer to the user-defined quantities.

3. CFD Simulation

3.1. CFD Model

Figure 4a,b illustrate the overall calculation model with and without the shroud, regardless of the influence of the meshing pinion, the shape of the gearbox, shaft, bearing, and other structures on the windage power loss. Table 1 illustrates the main parameters of the face gear. Figure 4c demonstrates the cross-sectional shape of the shroud. In this paper, CFD simulate the phenomenon of the face gear rotating in air and the windage loss of each tooth is completely consistent, so the periodic boundary condition (PBC) was adopted to simplify the calculation model and shorten the solution time [5,6,19], as shown in Figure 4c, where c_1, c_2, and c_3 represent the distance between the shroud and the gear body of the addendum direction, the outer radius direction, and the inner radius direction, respectively.

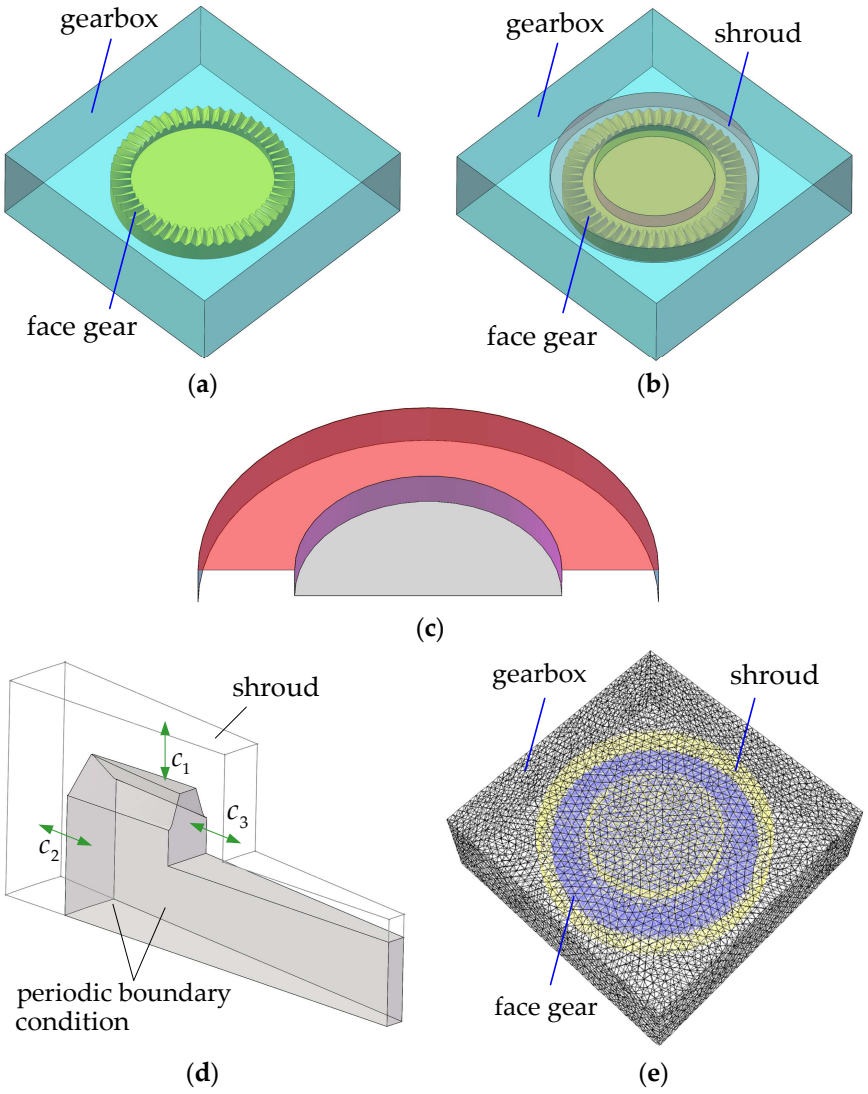

Figure 4. (**a**) Overall calculation CFD model without shroud; (**b**) overall calculation CFD model with shroud; (**c**) cross-section of the shroud; (**d**) PBC calculation CFD model; and (**e**) mesh model with shroud.

Table 1. Main parameters of the face gear.

Parameters	Values
Teeth number of the face gear	51
Module (mm)	2.5
Pressure angle (°)	25
Shaft angle (°)	90
Inner radius of the face gear (mm)	64.0
Outer radius of the face gear (mm)	82.0

The computational domain was divided into tetrahedral meshes in the Workbench-Mesh. Figure 4d presents the final mesh model, where the maximum skewness, maximum aspect ratio, average orthogonal quality, and the mesh quality were 0.814, 24.419, 0.702, and 0.303, respectively. Since the SST $k-\omega$ model was adopted in the simulation, the mesh criterion requirement $y+ < 5$ was necessary to adequately use the turbulent model. In the post-processing, the dimensionless wall parameter $y+$ obtained was within the range from 0.159 to 1.32, validating the correctness of the mesh model. Furthermore, to improve the accuracy and reliability of the simulation results, a grid independence test was performed in this paper. Table 2 lists the number of mesh elements in six cases. Windage loss is the focus of this paper and static pressure is an important factor to evaluate the windage loss of gears according to the existing literature [14], so the static pressure distribution on any symmetrical surface passing through the axis of the face gear is taken as the standard of the grid independence test and Figure 5 illustrates the simulation results. As seen from the figure, when the number of mesh elements reaches case 4, the static pressure can be considered stable. Therefore, the number of mesh elements in all subsequent simulations was controlled at approximately 1.1 million.

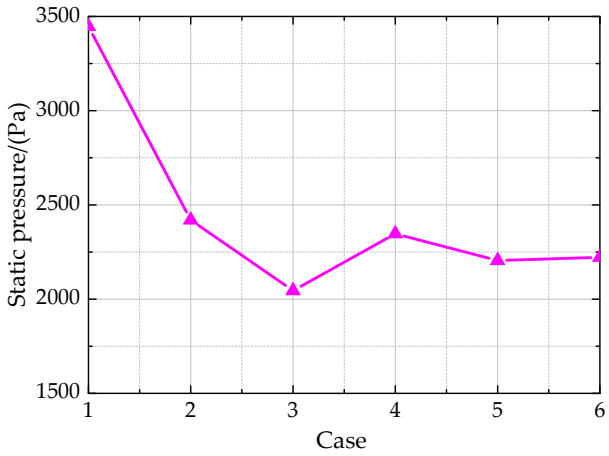

Figure 5. Static pressure under the six cases of total mesh elements.

Table 2. Cases of mesh elements.

Case	Total Mesh Elements
1	412,752
2	657,916
3	895,308
4	1,157,804
5	1,305,782
6	1,549,800

3.2. Main Settings of Simulation

Despite the influence of other factors, the windage phenomenon of a face gear rotating in the air can be considered as a steady-state process, so a steady-state solver based on the pressure

solver was adopted in this paper. Considering the synergy between different computing domains, the multi-reference frame (MRF) was applied to simulate the windage phenomenon. To obtain a more accurate solution, the second-order windward methods of momentum, turbulent kinetic energy, and turbulent dissipation rate were adopted for the spatial discretization. Furthermore, the standard simple algorithm can be used for pressure velocity coupling and the influence of gravity cannot be ignored. According to the existing research [39,40], this work makes the following reasonable assumptions:

- The air around the face gear was assumed to be pure and Mach number of the air was less than 0.3; that is, it was incompressible, and the density and viscosity were 1.225 kg/m^3 and 0.01834 kg/m · s, respectively.
- When the residuals of the continuity equation and the momentum equation were less than 0.0001, the convergence state can be considered.
- All moving walls were supposed to be unsmooth with a roughness of 3.2 µm.

4. Results Analysis

4.1. Analysis of the Gear Speed and Shroud

To observe the windage phenomenon more clearly, two planes named as Section 1 and Section 2 were made on the gear body, as shown in Figure 6, where Section 1 was the middle plane that bisects the tooth space and passes though the axis, and Section 2 was parallel to the surface of the addendum and the distance to the addendum was 1 m (m is the module of the face gear).

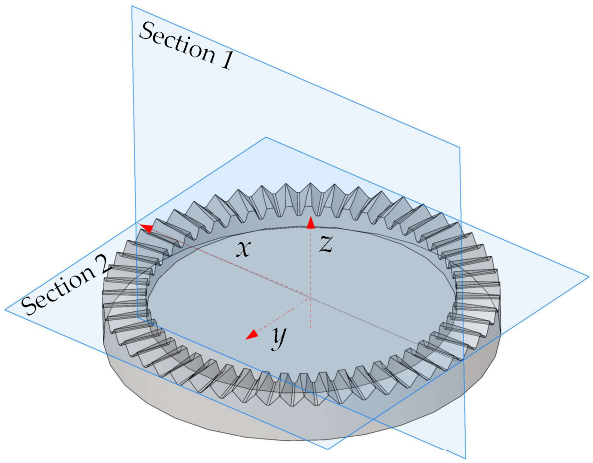

Figure 6. Description of Sections 1 and 2.

Figure 7 demonstrates the velocity contours of the face gear on Section 1 without and with a shroud, respectively, and the initial shroud position is $c_1 = 10$ mm, $c_2 = 10$ mm, and $c_3 = 10$ mm. According to Figure 7a, it can be seen that the fluid velocity on both sides of the tooth surface was inconsistent, which was caused by the single rotating face gear. The velocity on the side along the rotation direction was greater than that on the other side, resulting in different pressure on both sides and causing energy loss. It can also be seen that the teeth were the main source of windage loss. When the gear with a shroud rotates in the air (as shown in Figure 7b), the fluid velocity near the face gear teeth was significantly reduced and the extreme value of velocity was mainly concentrated on the edge part of the shroud. Moreover, from the pressure contours of face gears without and with a shroud, which are illustrated in Figure 8, it can be concluded that the extreme value of pressure without a shroud was mainly concentrated on the tooth surface, and the pressure of the windward tooth face was larger than that of the leeward tooth surface. This pressure was obviously reduced after the shroud

was added to the face gear. Thus, it can be concluded that the addition of a shroud to the face gear can effectively reduce the windage power loss.

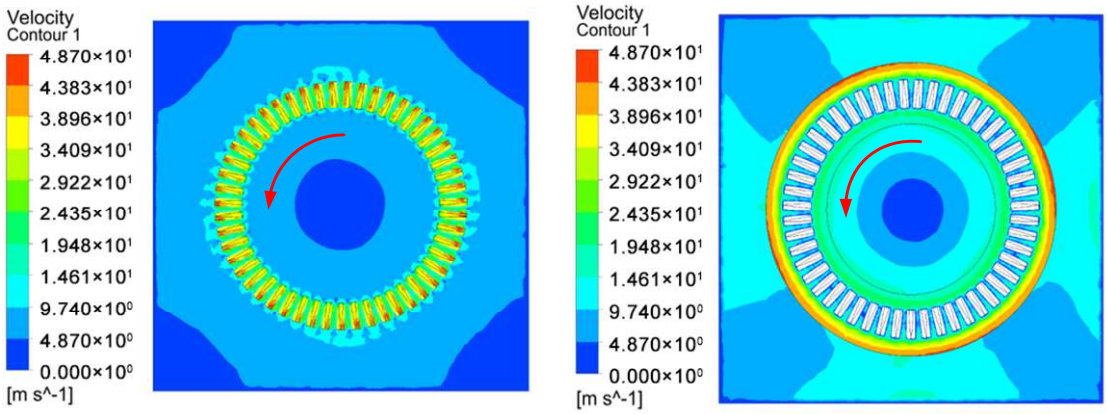

(**a**) (**b**)

Figure 7. Velocity contours on Section 1: (**a**) without shroud; (**b**) with shroud.

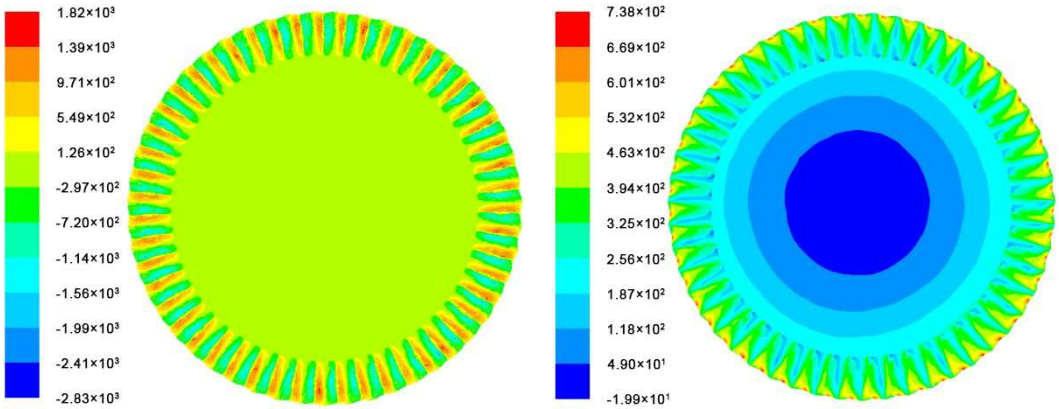

(**a**) (**b**)

Figure 8. Pressure contours of the single face gear: (**a**) without shroud; (**b**) with shroud.

Static pressure has been proven to be an important factor in the evaluation of windage power loss in open literature, so the static pressure on Section 1 was also adopted to study windage loss of the face gear. The *x*-axis (shown in Figure 6) coordinates ranged from 0.052 to 0.093 based on the initial position of the shroud in the inner radius direction and the outer radius direction. The range was divided into 42 regions with the interval length of 0.001, and the average value of all pressures in each region was used to represent the pressure of the region by the rounding-off method. Figures 9 and 10 illustrate the static pressure and the fluid velocity on Section 1 along the *x*-axis with and without shroud, respectively. According to Figure 9, rotational speed acts as an important role in the windage loss of face gears. It can be concluded that the higher the gear speed is, the greater the static pressure difference and the fluid velocity difference on both sides of the gear teeth, that is, the greater the windage power loss. Additionally, static pressure and velocity had almost no change until close to the gear teeth, which further verifies that the gear teeth were the main source of windage power loss instead of the gear plate. For the face gear with shroud, the gear speed also significantly affected the windage power loss, and the same conclusion applies; that is, that the greater the gear speed is, the greater the windage loss, and the maximum static pressure appears near the inner radius and outer radius. It is also known from Figures 9 and 10 that the shroud had a great influence on the windage power loss. Under the condition of the same gear speed, the static pressure and fluid velocity of Section 1 were significantly reduced

after the shroud was applied on the face gear, which greatly reduced the windage power loss. Thus, it is of practical significance to investigate the windage power loss of the face gear with the shroud.

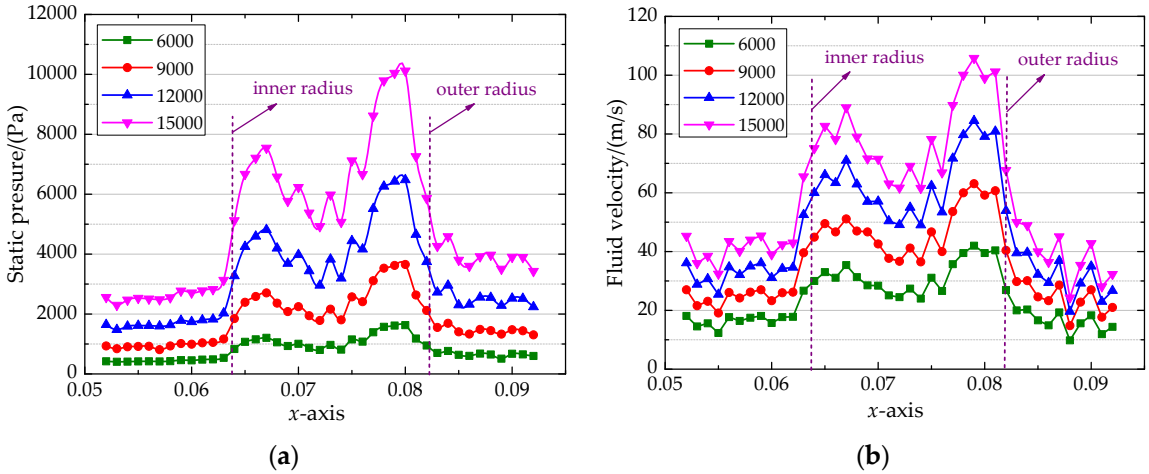

Figure 9. The distribution without shroud at different rotational speeds of: (**a**) static pressure; (**b**) fluid velocity.

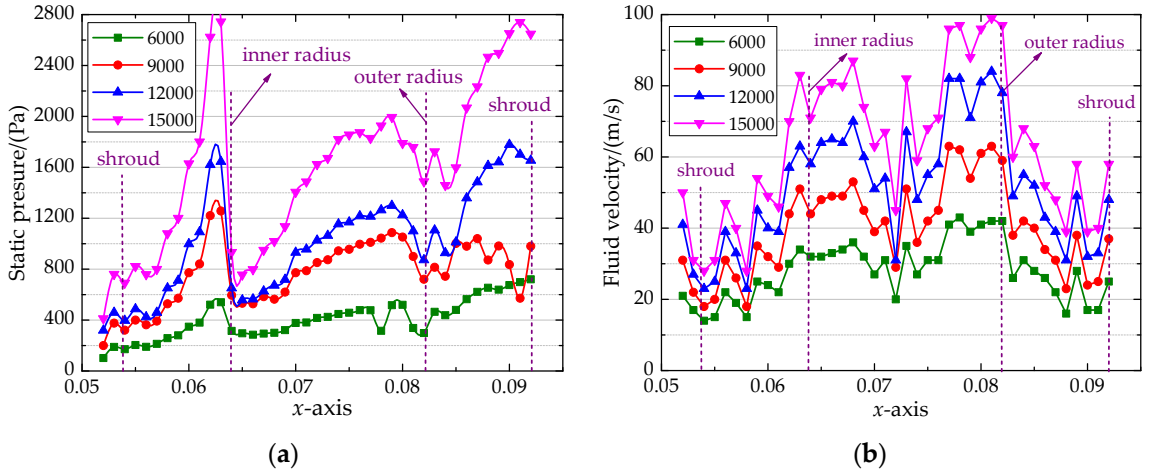

Figure 10. The distribution with shroud at different rotational speeds of: (**a**) static pressure; (**b**) fluid velocity.

As seen from Figure 4d, the shroud mainly covers three directions of the face gear, including the addendum direction c_1, the inner radius direction c_2, and the outer diameter direction c_3. To determine the best placed position of the shroud, the influence on the windage power loss of the distance from the shroud to the gear in each of the three directions was investigated in this work.

Meanwhile, Figure 11a demonstrates the trend of the power losses without and with a shroud at different speeds. It can be concluded that the power increased with the gear speed increasing, and the shroud can significantly reduce the power loss. The inertial and viscosity contributions to the total power losses without and with a shroud are illustrated in Figure 11b,c, respectively. As can be seen, inertia was the main contribution to the windage power loss rather than viscosity, and this contribution increased with the increase in gear speed. Furthermore, after adding a shroud, the inertial contribution decreased significantly.

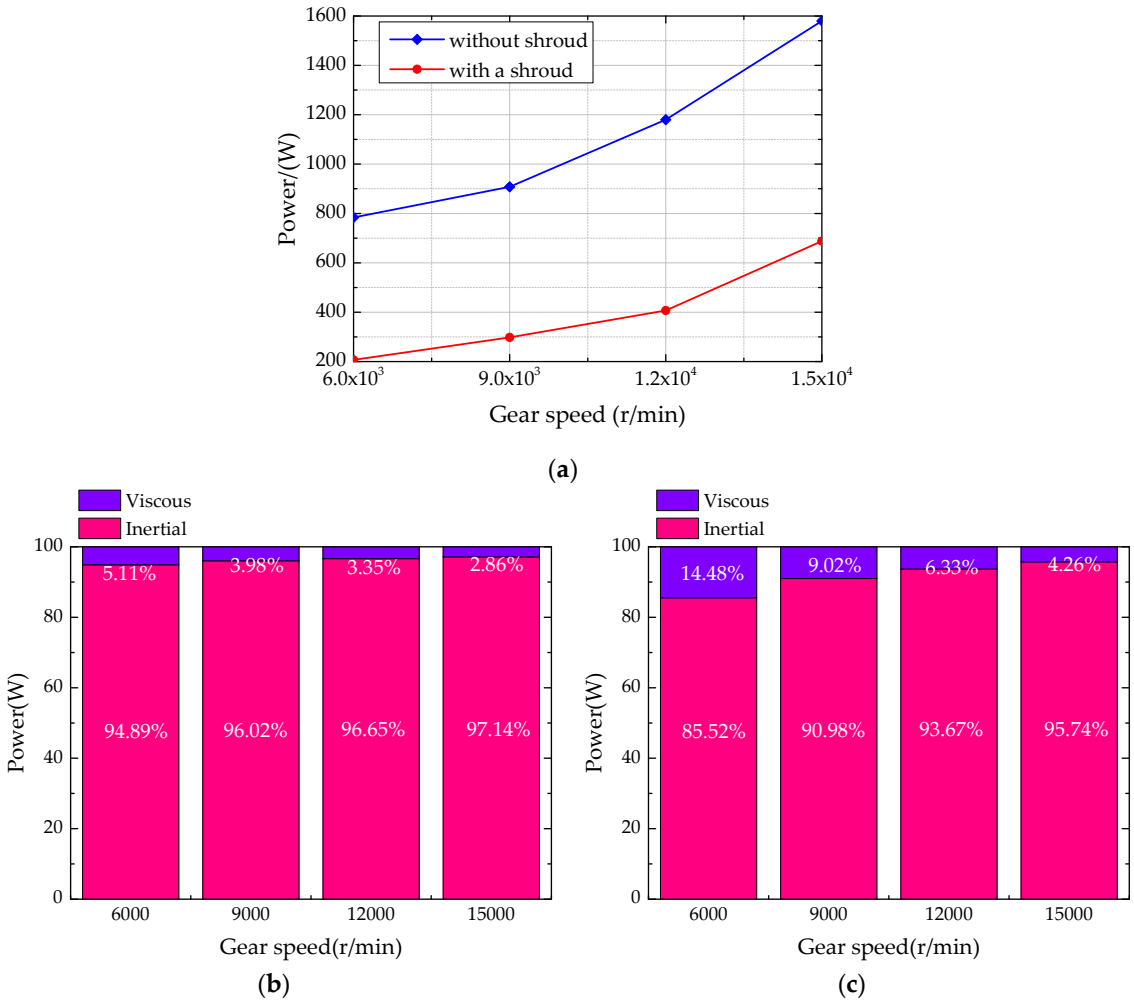

Figure 11. (**a**) The trend of the power losses without and with a shroud at different speeds: (**b**) the inertial and viscosity contributions to the total power losses without a shroud; (**c**) the inertial and viscosity contributions to the total power losses with a shroud.

4.2. Analysis of the Distance c_1

According to the open literature, four values for the distance c_1 were set as 2.5 mm, 5 mm, 7.5 mm, and 10 mm, and the other two distances c_2 and c_3 were set to 10 mm. For ensuring the accuracy and credibility of the simulation results, c_1 was the only independent variable in the simulations, and all simulation settings were consistent. With the monitors set to 0.0001 and the simulation convergent, the static pressure contours on Section 1, with the four distance values, are demonstrated in Figure 12a–d, respectively. As can be seen from Figure 12, the static pressure on Section 1 was obviously different with the different values of the distance c_1. As the distance decreased, the static pressure on Section 1 first decreased and then increased, when the distance was set to 7.5 mm, the static pressure was minimized, which means that the shroud worked better at this distance.

To observe the change rules of the static pressure more clearly, the curve diagram shown in Figure 13 was made. It can be concluded that the maximum static pressure occurred near the outer shroud and inner radius, and it can be considered that the shroud can reduce the windage loss, but the flowing air also causes energy loss near the shroud. Therefore, it is not suggested that the closer the shroud is to the addendum, the better. As the distance decreased, the static pressure on Section 1 decreased first and then increased, which is consistent with the conclusion obtained from the static pressure contours, and the two were mutually verified.

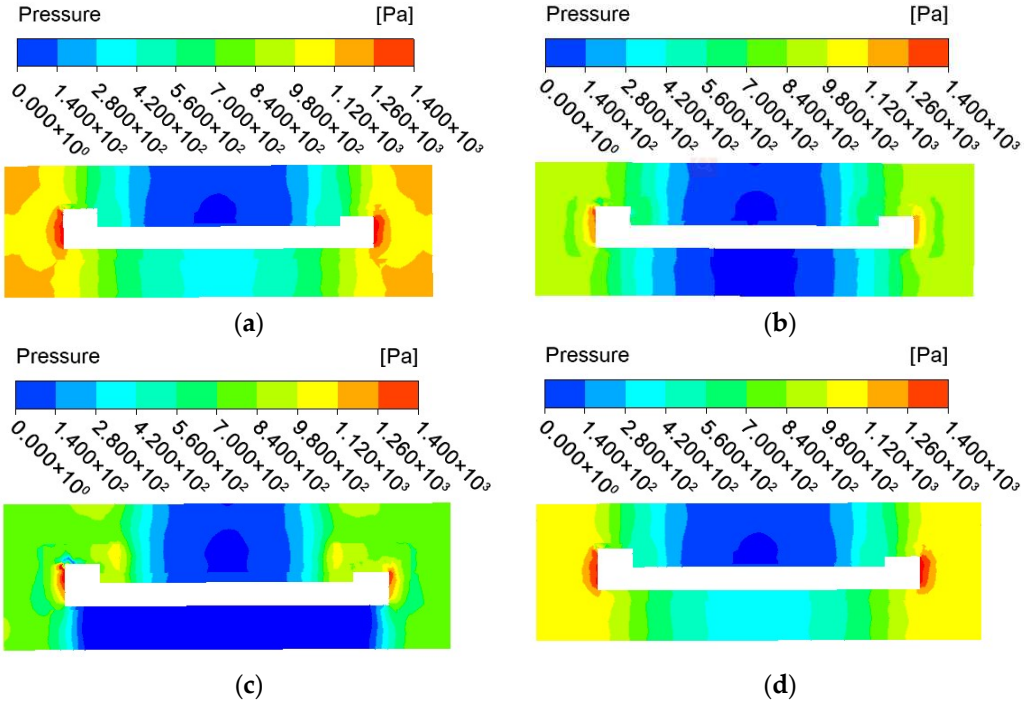

Figure 12. Static pressure contours on Section 1 under different values of c_1: (**a**) 2.5 mm; (**b**) 5 mm; (**c**) 7.5 mm; (**d**) 10 mm.

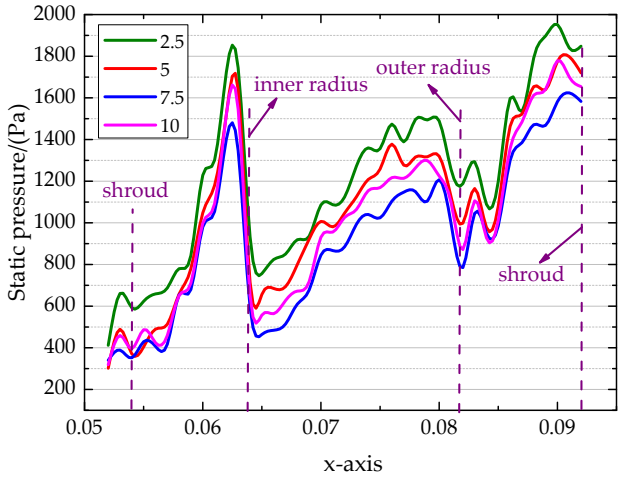

Figure 13. Change rules of static pressure along the *x*-axis under different values of the distance c_1.

4.3. Analysis of the Distance c_2

According to Section 3.2, when the distance c_1 was set as 7.5 mm, the minimum static pressure and the minimum windage power loss were obtained. Therefore, the distance c_2 was studied on the basis of $c_1 = 7.5$ mm. The four values of the distance c_2 were optimized to be 2.5 mm, 5 mm, 7.5 mm, and 10 mm. Moreover, the distance c_3 is kept unchanged. Finally, the static pressure on Section 1 is shown in Figure 14. It can be concluded that as the distance c_2 decreased, the static pressure on Section 1 also decreased, especially in the vicinity of the teeth, which means that the windage power loss also decreased.

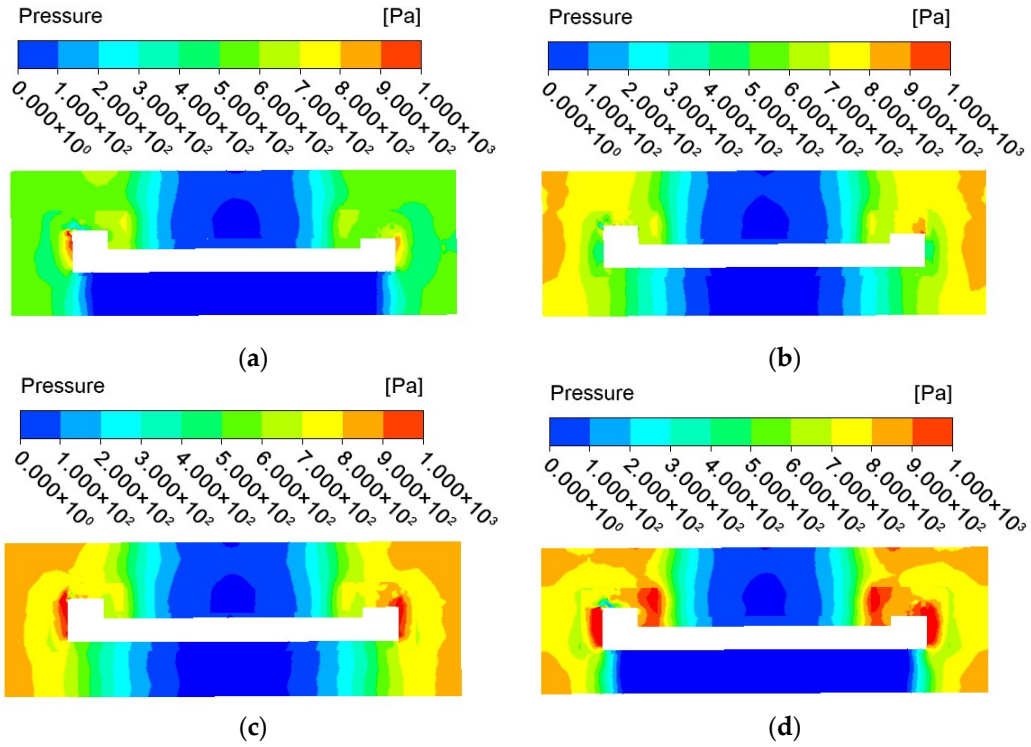

Figure 14. Static pressure contours on Section 1 under different values of c_2: (**a**) 2.5 mm; (**b**) 5 mm; (**c**) 7.5 mm; (**d**) 10 mm.

Similarly, Figure 15 illustrates the change rules of static pressure on Section 1. It can be observed that, as the distance c_2 decreased, the static pressure on Section 1 along the x-axis also decreased, which means that the windage power loss decreased. Moreover, the smaller the distance c_2, the smaller the x-coordinate value of the maximum pressure close to the outer radius of the gear body. To summarize, the following conclusion can be drawn: the smaller the distance between the shroud and the outer radius of the gear body, the smaller the windage power loss. Therefore, in practical applications, this distance can be shortened as much as possible for achieving higher transmission efficiency and lower energy loss.

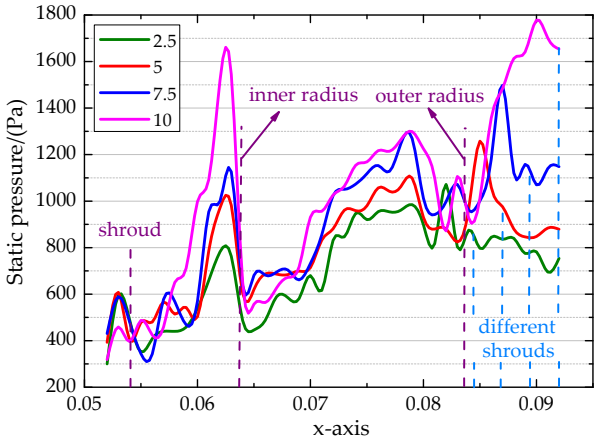

Figure 15. Change rules of static pressure along the x-axis under the different values of the distance c_2.

4.4. Analysis of the Distance c_3

Based on the above research, the minimum static pressure and the minimum windage loss were obtained in the case of $c_1 = 7.5$ mm and $c_2 = 2.5$ mm. Therefore, these two values were also used

in the study of the distance c_3. Similarly, the parameter c_3 was optimized to 2.5 mm, 5 mm, 7.5 mm, and 10 mm, and the static pressure on Section 1 is illustrated in Figure 16 under the condition that all simulation settings are consistent. From Figure 16, it can be seen that as the distance c_3 decreased, the static pressure on Section 1 also decreased, which means that the windage power loss also decreased. Moreover, the extreme values of static pressure appear near the teeth.

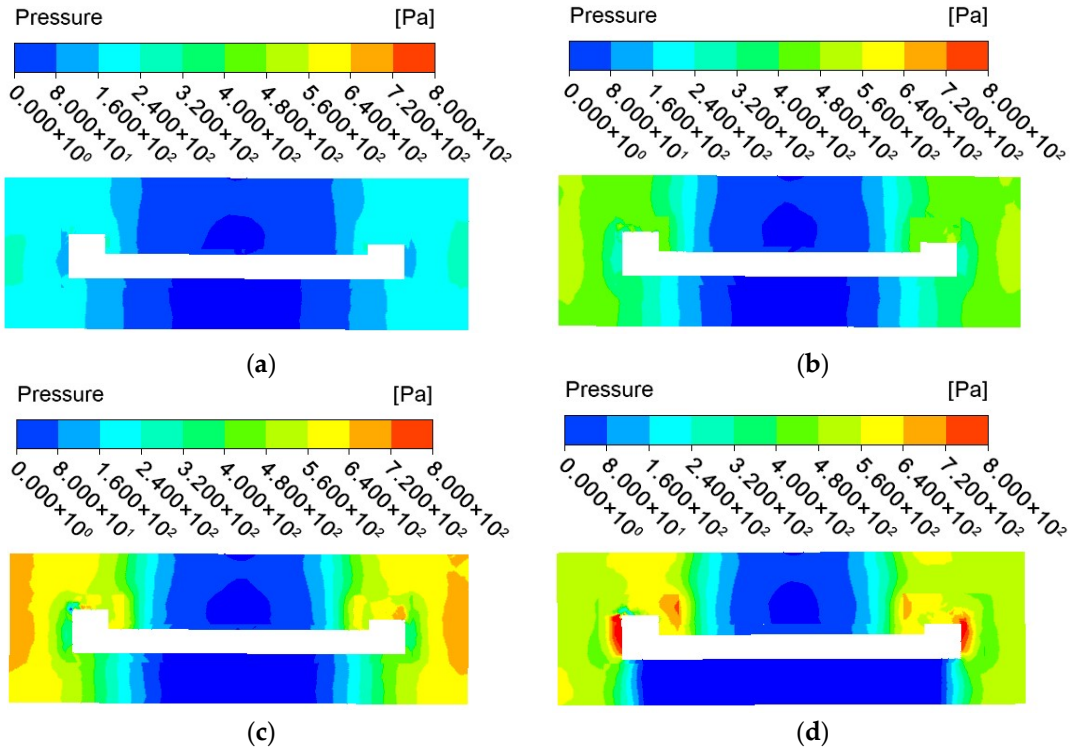

Figure 16. Static pressure contours on Section 1 under different values of c_3: (**a**) 2.5 mm; (**b**) 5 mm; (**c**) 7.5 mm; (**d**) 10 mm.

Figure 17 demonstrates the change rules of static pressure on Section 1 under the different values of the distance c_3. It can be observed that, with the decrease of the distance c_3, the static pressure on Section 1 also decreased, which means that the windage power loss decreased. Furthermore, the smaller the distance c_3, the smaller the x-coordinate value of the maximum static pressure close to the outer radius of the gear body. Hence, in practical applications, the distance from the shroud to the inner radius of the gear body can be reduced as much as possible, similar to the conclusion obtained from Section 4.3.

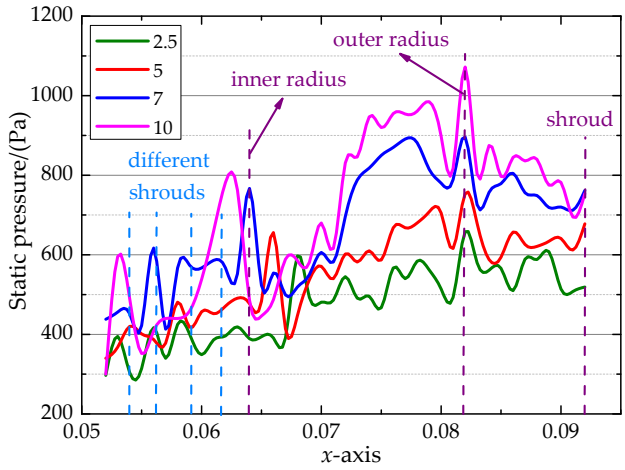

Figure 17. Change rules of static pressure along the x-axis under the different values of the distance c_3.

4.5. Practical Applications

Figure 18 summarizes the corresponding power values in the previous CFD simulation groups, where Numbers 1–10 represent Figures 12a–d, 14a–c and 16a–c. As can be seen, the windage power loss in Number 8 was the lowest, that is $c_1 = 7.5$ mm, $c_2 = 2.5$ mm, and $c_3 = 2.5$ mm.

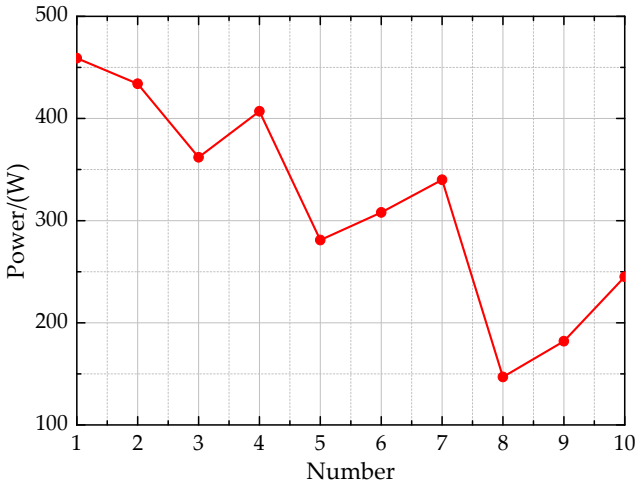

Figure 18. The trend of the corresponding power values in the previous CFD simulation groups.

For a face gear drive, the shape and arrangement of the shroud needs to take the meshing pinion into consideration comprehensively. According to the above study on the windage loss of the face gear, the distance from the shroud to the gear body in the inner radius and outer radius direction should be reduced as far as possible, and the distance between the shroud and the gear addendum should be appropriately reduced. For the meshed pinion, the shroud can be reasonably arranged according to the existing research [21], and the final recommended shape of the shroud is shown in Figure 19.

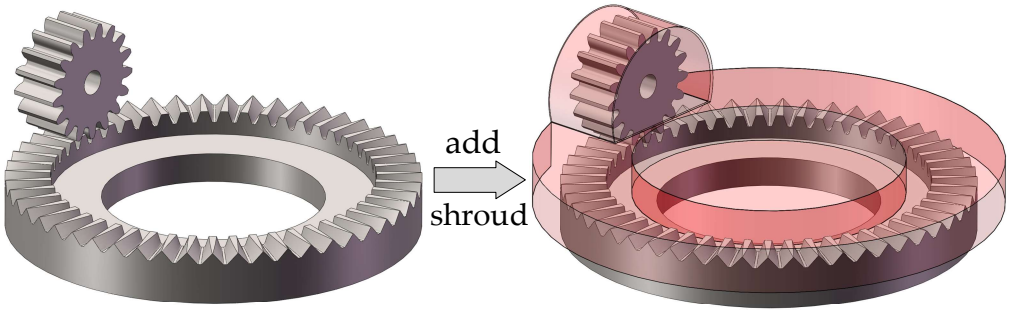

Figure 19. Recommended shroud for face gear drive.

5. Conclusions

To reduce the energy loss of the face gear drive, the windage phenomenon of the face gear with and without a shroud was investigated based on a CFD model; the major conclusions drawn from this work are described below:

1. The steering of the face gear has no effect on the windage losses. The teeth are the main source of windage loss instead of the gear plate. Gear speed plays a significant role in the windage loss of the face gear, and the greater the gear speed is, the greater the windage loss will be.
2. The shroud can significantly reduce the windage losses of face gears. The distance from the shroud to the gear body in three directions has an effect on the windage losses, including the distance from the shroud to the tooth addendum, the distance from the shroud to the outer radius and the distance between the shroud and the inner radius.

3. The distance from the shroud to the face gear addendum should not be as small as possible. As the distance decreases, the windage power loss decreases first and then increases. For the distances between the shroud and the outer radius and inner radius, the smaller the distance values are, the smaller the windage power loss—that is, the greater the efficiency of the face gear drive. Furthermore, the shroud that effectively reduces the windage loss of the face gear drive is recommended.

Author Contributions: All listed authors have contributed to this research. Y.D. proposed the research ideas and guided the work; F.M. and Y.D. wrote this manuscript and performed the numerical simulations. X.Z. and J.J. put forward some suggestions.

Funding: This research was funded by the National Defense Preliminary Research Project of China grant number KY-44-2018-0219.

Acknowledgments: We would like to express our thanks to the editors of *Energies* and the anonymous reviewers for their work in processing this article.

Conflicts of Interest: The authors declare no conflict of interest.

References

1. Feng, G.; Xie, Z.; Zhou, M. Geometric design and analysis of face-gear drive with involute helical pinion. *Mech. Mach. Theory* **2019**, *134*, 169–196. [CrossRef]
2. Saribay, Z.B.; Bill, R.C.; Smith, E.C.; Rao, S.B. Geometry and Kinematics of Conjugate Meshing Face-Gear Pairs. *J. Am. Helicopter. Soc.* **2017**, *62*, 1–10. [CrossRef]
3. Hu, Z.H.; Tang, J.Y.; Chen, S.Y.; Sheng, Z.H. Coupled translation-rotation vibration and dynamic analysis of face geared rotor system. *J. Sound Vib.* **2015**, *351*, 169–196. [CrossRef]
4. Dai, Y.; Ma, F.; Zhu, X.; Su, Q.; Hu, X. Evaluation and Optimization of the Oil Jet Lubrication Performance for Orthogonal Face Gear Drive: Modelling, Simulation and Experimental Validation. *Energies* **2019**, *12*, 1935. [CrossRef]
5. Pallas, S.; Marchesse, Y.; Changenet, C.; Ville, F.; Velex, P. Application and validation of a simplified numerical approach for the estimation of windage power losses in spur gears. *Comput. Fluids* **2013**, *84*, 39–45. [CrossRef]
6. Fondelli, T.; Andreini, A.; Facchini, B. Numerical Investigation on Windage Losses of High-Speed Gears in Enclosed Configuration. *AIAA J.* **2018**, *56*, 1910–1921. [CrossRef]
7. Dawson, P.H. Windage Loss in Larger High-Speed Gears. *Proc. Inst. Mech. Eng. Part. A Power Process. Eng.* **1984**, *198*, 51–59. [CrossRef]
8. Dawson, P.H. High-speed gear windage. *GEC Rev.* **1988**, *43*, 164–167.
9. Anderson, N.E.; Loewenthal, S.H.; Black, J.D. An Analytical Method to Predict Efficiency of Aircraft Gearboxes. *J. Mech. Transm. Autom. Des.* **1984**, *108*, 424–432. [CrossRef]
10. Anderson, N.E.; Loewenthal, S.H. Efficiency of nonstandard and high contact ratio involute spur gears. *J. Mech. Transm. Autom. Des.* **1986**, *108*, 119–126. [CrossRef]
11. Diab, Y.; Ville, F.; Velex, P.; Changenet, C. Windage losses in high speed gears—Preliminary experimental and theoretical results. *J. Mech. Des.* **2004**, *126*, 903–908. [CrossRef]
12. Handschuh, R.F.; Hurrell, M.J. *Initial Experiments of High-Speed Drive System Windage Losses*; NASA TM-2011-216925; NASA: Washington, DC, USA, 2011.
13. Farrall, M.; Simmons, K.; Hibberd, S.; Young, C. Computational Investigation of the Airflow Through a Shrouded Bevel Gear. In Proceedings of the GT2005 ASME Turbo Expo 2005: Power for Land, Sea and Air, Reno-Tahoe, Nevada, NV, USA, 6–9 June 2005.
14. Eastwick, C.N.; Johnson, G. Gear Windage: A Review. *J. Mech. Des.* **2008**, *130*. [CrossRef]
15. Johnson, G.; Simmons, K.; Foord, C. Experimental Investigation into Windage Power Loss From a Shrouded Spiral Bevel Gear. In Proceedings of the GT2007 ASME Turbo Expo 2007: Power for Land, Sea and Air, Montreal, QC, Canada, 14–17 May 2007.
16. Hill, M.J.; Kunz, R.F.; Medvitz, R.B.; Handschuh, R.F.; Long, L.N.; Noack, R.W.; Morris, P.J. CFD Analysis of Gear Windage Losses: Validation and Parametric Aerodynamic Studies. *J. Fluid. Eng.* **2011**, *133*. [CrossRef]
17. Concli, F.; Gorla, C.; Torre, A.D.; Montenegro, G. Windage power losses of ordinary gears: Different CFD approaches aimed to the reduction of the computational effort. *Lubricants* **2014**, *2*, 162–176. [CrossRef]

18. Concli, F.; Gorla, C.; Della Torre, A.; Montenegro, G. Churning power losses of ordinary gears: A new approach based on the internal fluid dynamics simulations. *Lubr. Sci.* **2015**, *27*, 313–326. [CrossRef]
19. Pallas, S.; Marchesse, Y.; Changenet, C. A windage power loss model based on CFD study about the volumetric flow rate expelled by spur gears. *Mech. Ind.* **2012**, *13*, 317–323. [CrossRef]
20. Arisawa, H.; Nishimura, M.; Imai, H.; Goi, T. CFD Simulation for Reduction of Oil Churning Loss and Windage Loss on Aeroengine Transmission Gears. In Proceedings of the ASME Turbo Expo 2009, Orlando, FL, USA, 8–12 June 2009.
21. Voeltzel, N.; Marchesse, Y.; Changenet, C.; Ville, F.; Velex, P. On the influence of helix angle and face width on gear windage losses. *Proc. Inst. Mech. Eng. C-J. Mech.* **2016**, *230*, 1101–1112. [CrossRef]
22. Rapley, S.; Eastwick, C.; Simmons, K. The Application of CFD to Model Windage Power Loss from a Spiral Bevel Gear. In Proceedings of the GT2007 ASME Turbo Expo 2007: Power for Land, Sea and Air, Montreal, QC, Canada, 14–17 May 2007.
23. Marchesse, Y.Y.; Changenet, C.C.; Ville, F.F.; Velex, P.P. Investigations on CFD Simulations for Predicting Windage Power Losses in Spur Gears. *J. Mech. Des.* **2011**, *133*. [CrossRef]
24. Concli, F. Thermal and efficiency characterization of a low-backlash planetary gearbox: An integrated numerical-analytical prediction model and its experimental validation. *Proc. Inst. Mech. Eng. J-J. Eng.* **2016**, *230*, 996–1005. [CrossRef]
25. Concli, F.; Gorla, C.; Stahl, K.; Höhn, B.-R.; Michaelis, K.; Schultheiß, H.; Stemplinger, J.P. Load independent power losses of ordinary gears: Numerical and experimental analysis. In Proceedings of the 5th World Tribology Congress, Torino, Italy, 8–13 September 2013.
26. Delgado, I.R.; Hurrell, M.J. Baseline Experimental Results on the Effect of Oil Temperature on Shrouded Meshed Spur Gear Windage Power Loss. In Proceedings of the International Design Engineering Technical Conferences and Computers and Information in Engineering Conference, Cleveland, OH, USA, 6–9 August 2017.
27. Seetharaman, S.; Kahraman, A. A Windage Power Loss Model for Spur Gear Pairs. *J. Tribol. Trans.* **2010**, *53*, 473–484. [CrossRef]
28. Webb, T.; Eastwick, C.; Morvan, H. Parametric Modelling of a Spiral Bevel Gear Using CFD. In Proceedings of the Asme Turbo Expo 2010, Glasgow, Scotland, 14–18 June 2010.
29. Aktas, M.K.; Yavuz, M.A.; Ersan, A.K. Computational Fluid Dynamics Simulations of Windage Loss in a Spur Gear. In Proceedings of the ASME Turbo Expo 2018 Turbomachinery Technical Conference and Exposition, Oslo, Norway, 11–15 June 2018.
30. Concli, F.; Gorla, C. Numerical modelling of the churning power losses in planetary gearboxes: An innovative partitioning-based meshing methodology for the application of a computational effort reduction strategy to complex gearbox configurations. *Lubr. Sci.* **2017**, *29*, 455–474. [CrossRef]
31. Concli, F.; Della Torre, A.; Gorla, C.; Montenegro, G. A New Integrated Approach for the Prediction of the Load Independent Power Losses of Gears: Development of a Mesh-Handling Algorithm to Reduce the CFD Simulation Time. *Adv. Tribol.* **2016**, *2016*, 2957151. [CrossRef]
32. Winfree, D.D. Reducing Gear Windage Losses from High Speed Gears and Applying These Principles to Actual Running Hardware. In Proceedings of the ASME 2013 International Design Engineering Technical Conferences and Computers and Information in Engineering Conference, Portland, OR, USA, 4–7 August 2013.
33. Litvin, F.L.; Fuentesm, A.; Howkins, M. Design, generation and TCA of new type of asymmetric face-gear drive with modified geometry. *Comput. Methods Appl. Mech. Eng.* **2001**, *190*, 5837–5865. [CrossRef]
34. Litvin, F.L.; Fuentesm, A.; Zanzim, C. Face-gear drive with spur involute pinion: Geometry, generation by a worm, stress analysis. *Comput. Methods Appl. Mech. Eng.* **2002**, *191*, 2785–2813. [CrossRef]
35. Guingand, M.; Vaujany, J.P.; Jacquin, C.Y. Quasi-static analysis of a face gear under torque. *Comput. Methods Appl. Mech. Eng.* **2005**, *194*, 4301–4318. [CrossRef]
36. Wang, Y.; Song, G.; Niu, W.; Chen, Y. Influence of oil injection methods on the lubrication process of high speed spur gears. *Tribol. Int.* **2018**, *121*, 180–189. [CrossRef]
37. Dai, Y.; Wu, W.; Zhou, H.; Zhang, J.; Ma, F. Numerical Simulation and Optimization of Oil Jet Lubrication for Rotorcraft Meshing Gears. *Int. J. Simul. Model.* **2018**, *17*, 318–326. [CrossRef]
38. Hu, X.; Jiang, Y.; Luo, C.; Feng, L.; Dai, Y. Churning power losses of a gearbox with spiral bevel geared transmission. *Tribol. Int.* **2019**, *129*, 398–406. [CrossRef]

39. Franco, C.; Carlo, G. Numerical modeling of the power losses in geared transmissions: Windage, churning and cavitation simulations with a new integrated approach that drastically reduces the computational effort. *Tribol. Int.* **2016**, *103*, 58–68.
40. Massini, D.; Fondelli, T.; Andreini, A.; Facchini, B.; Tarchi, L.; Leonardi, F.F. Experimental and Numerical Investigation on Windage Power Losses in High Speed Gears. *J. Eng. Gas Turbines Power* **2018**, *140*. [CrossRef]